Manuscript:

Exploring the application of TEX_{86} and the sources of organic matter in the Antarctic coastal region

Ana Lúcia L. Dauner [a,b,1,*], B. David A. Naafs [c], Richard D. Pancost [c,d,e], César C. Martins [a,*]

[a] Center for Marine Studies, Federal University of Paraná, 83255-976 Pontal do Paraná, PR, Brazil

[b] Graduate Program in Coastal and Oceanic Systems (PGSISCO) of the Federal University of Paraná, 83255-976 Pontal do Paraná, PR, Brazil

[c] Organic Geochemistry Unit, School of Chemistry, University of Bristol, Bristol BS8 1TS, UK

[d] Cabot Institute for the Environment, University of Bristol, Bristol BS8 1UJ, UK

[e] School of Earth Sciences, University of Bristol, Bristol BS8 1RL, UK

[1] Current institution: Environmental Change Research Unit (ECRU), Ecosystems and Environment Research Programme, Faculty of Biological and Environmental Sciences, 00014, University of Helsinki, Helsinki, Finland.

* Corresponding author: anadauner@gmail.com (A.L.L. Dauner)
ccmart@ufpr.br (C.C. Martins)

Highlights

> Five GDGT-based calibrations were tested against reanalysis temperatures.

> The best fit was obtained using with a quadratic calibration.

> The GDGT-based sea surface temperature (SST) represented the Oct/Nov/Dec season.

> Organic matter input was controlled mainly by SST, precipitation and glacier retreat.

Abstract

Isoprenoidal glycerol dialkyl glycerol tetraethers (isoGDGTs) are archaeal biomarkers. In many settings, the degree of cyclization of isoGDGTs is correlated with temperature, forming the basis of the TEX_{86} paleothermometer that is widely used to reconstruct sea surface temperature (SST) across a range of time scales. However, the application of TEX_{86} to the polar regions is relatively limited and there is currently no consensus on which calibration is best suited for polar environments. In addition, application of TEX_{86} to the polar regions is complicated by uncertainty regarding the source of organic matter input in coastal polar environments. We tested five different calibrations for TEX_{86} in marine sediments from the Antarctic coastal region of Admiralty Bay near King George Island, using four short cores that span the second half of the 20th century. We also explored the possible sources of organic matter in these cores using sterol biomarkers. Best results for TEX_{86} were obtained using a quadratic calibration. The TEX_{86} signal presented a strong seasonal signal and best matched reanalysis temperatures of the austral spring season (Oct/Nov/Dec). The most abundant compounds observed in the sediments were the sterols cholest-5-en-3β-ol and 24-ethylcholest-5-en-3β-ol, the fatty alcohols C_{16} and phytol, and isoGDGT-0, indicating a dominant marine origin of the organic matter. Differences in their vertical distributions suggests that some compounds (such as cholest-5-en-3β-ol and phytol) may have had different sources over the evaluated period. Together our results indicate that TEX_{86} can be used to reconstruct SSTs in the Antarctic coastal region.

Keywords: GDGT, sterol, sea surface temperature; organic matter; Admiralty Bay.

1. Introduction

Several biomarkers-based proxies have been developed for the reconstruction of sea surface temperature and organic matter (OM) production in the marine environment (Volkman, 2006; Eglinton and Eglinton, 2008; Schouten et al., 2013). A main focus has been on the isoprenoidal glycerol dialkyl glycerol tetraethers (isoGDGTs) produced by Archaea. The degree of cyclization of isoGDGTs is correlated with temperature in both laboratory cultures (De Rosa et al., 1980) and natural samples (Schouten et al., 2002; Kaur et al., 2015). This forms the basis for the TEX_{86} paleothermometer (Schouten et al., 2002, 2013) that is widely used to reconstruct sea surface temperature (SST) across a range of time scales and as far back as the early Jurassic (e.g. Hertzberg et al., 2016; Robinson et al., 2017; Petrick et al., 2018). However, other factors can also influence the degree of cyclization of isoGDGTs under specific conditions (Pearson et al., 2004; Elling et al., 2015).

TEX_{86} can be particularly useful in locations where other proxies cannot be easily applied, such as in the Southern Ocean and Antarctic shelf (Ho et al., 2014). However, the application of TEX_{86} to the polar regions is still relatively limited and there is currently no consensus on which calibration is best suited for polar environments (Etourneau et al., 2013; Tierney and Tingley, 2014; Park et al., 2019). There are only a few studies that test the application of TEX_{86} calibrations in the Antarctic and Southern Ocean environments and most of them used sediments recovered from the open ocean (e.g. Ho et al., 2014 and Fietz et al., 2016). An exception is the study by Jaeschke et al. (2017) that analyzed surface sediment samples encompassing a large range of latitudes (between 36° S and 68° S), including the Southern Ocean. Nevertheless, only a few of them were located below the Antarctic Polar Front, and all samples from the polar region (> 60° S) overestimated SST by up to 6 °C. The authors suggested the influence of seasonality and terrestrial input as explanations for this large bias in their polar samples.

Some studies adapted pre-existing calibrations to develop regional models for the Antarctic polar environment. Shevenell et al. (2011) modified the calibration model of Schouten et al. (2002) and suggested a regional calibration for the Antarctic Peninsula. More recently, Park et al. (2019) studied the seasonal effect on the GDGT-based thermometry from the Antarctic Polar Front. Based on the global calibration proposed by Kim et al. (2010), they concluded that there is a nonlinear relationship between TEX_{86}^{L} and SST, and proposed a quadratic calibration for Antarctic environments south of 50° S.

However, a thorough assessment of the performance of these calibrations to the Antarctic environment is so far lacking.

In addition to the choice of the calibration method, the TEX_{86}^{L} –based SST reconstructions can also be affected by environmental conditions other than temperature, as mentioned earlier. Some studies identified that high productive regions and/or periods may affect the SST reconstruction (Hurley et al., 2018; Park et al., 2018). Although several studies have used biomarkers to reconstruct marine productivity and identify the sources of OM in Antarctic marine sediments (Huang et al., 2011; Wisnieski et al., 2014; Ceschim et al., 2016), none of the calibration studies in the Antarctic region evaluated the effect of variations in the OM productivity in the TEX_{86}^{L} –based SST paleothermometry.

In this context, understanding the environmental forcing and marine biogeochemical processes in polar environments involving the distribution and composition of sedimentary OM in general - and isoGDGT distributions specifically - is of high priority, and potentially able to assist in the understanding of local environmental changes (Shetye et al., 2017; Henley et al., 2019). The main objective of this work is to evaluate the OM character and sources, isoGDGT distributions and the performance of the TEX_{86} proxy in several short sediment cores from Admiralty Bay, located in the Sub-Antarctic sector, that span the second half of the 20th century. To evaluate the performance of the TEX_{86} proxy, several existing calibrations of the GDGT-based paleothermometer were tested to reconstruct sea surface temperature and compared to the available reanalysis record.

2. Study Area

Admiralty Bay is a glacial fjord, centrally located within King George Island (KGI), in the western region of the Antarctic Peninsula (Fig. 1). The island is mostly formed of volcanic rocks of Late Cretaceous to Early Terciary (Paleocene - Oligocene) ages, which are related to the subduction of the SE-Pacific oceanic crust underneath the Antarctic Continent (Smellie et al., 1984; Machado et al., 2001). Mafic volcanic rocks (i.e. basalts, basalt-andesites and andesites) are the dominant lithologies. Rhyiolite and dacite are less abundant (Machado et al., 1998).

In 1999, the KGI was more than 90% covered by ice fields, and the ice-free areas were concentrated along the coast (Simões et al., 1999). Due to regional warming, several glaciers have now retreated out of the sea. Between 2000 and 2008, the loss amounted to about 20 km^2, about 1.6% of the total area of the island (Rückamp et al., 2011). The

Admiralty Bay has an area of ca. 120 km^2, and it is composed of three branches: Ezcurra Inlet (E.I.) to the south-west, Mackellar Inlet (Mk.I.) to the north, and Martel Inlet (Mt.I.) to the north-east (Rakusa-Suszczewski, 1995). The water depth varies from shallow water up to 530 m deep, with an average depth of ca. 200 m (Rakusa-Suszczewski, 1995).

Surface sediments are heterogeneous, displaying coarse sediments (gravel and sand) mainly at the external and central parts of the bay (Fávaro et al., 2011). Ezcurra and Mackelar inlets display great heterogeneous grain size spatial distribution with sand content ranging between 6 and 60%. Sediments from Martel Inlet are predominantly composed of silt and clay fractions with percentages higher than 70% (Martins et al., 2005; Berbel and Braga, 2014).

The observed mean annual air temperature on the KGI was - 2.5 C° between 1948 and 2011 (Kejna et al., 2013). During austral Summer and also regularly during the Spring and Autumn months, air temperatures rise to well above freezing (Rückamp et al., 2011). Winds constitute a main meteorological feature and they influence the ablation rates, the surface energy fluxes (and therefore, the air temperatures), the water circulation and the resuspension of previously deposited material in the area (Braun et al., 2001, 2004; Pichlmaier et al., 2004). The precipitation on KGI is characterized by substantial interannual variability (Kejna et al., 2013) and affects the water column stratification and the resuspension of previously deposited material (Pichlmaier et al., 2004).

Hydrological conditions in Admiralty Bay are mainly driven by the exchange of water with the Bransfield Strait, freshwater runoff, and local processes in the fjord. The water flow can be described as tidal currents and superimposed wind driven currents (Robakiewicz and Rakusa-Suszczewski, 1999). The influence of wind and tidal variations on circulation is more intense in shallow areas, especially at the western side of the bay (Robakiewicz and Rakusa-Suszczewski, 1999) where wind plays an important role in upwelling that drives primary production (Brandini and Rebello, 1994). Freshwater runoff influences water column turbidity through the suspension of soft sediments in the region (Pichlmaier et al., 2004), and this runoff, enriched with guano and fragments of macroalgae, can be an important source of OM and nutrients to the bay (Nędzarek, 2008).

3. Material and Methods

3.1. Sampling

Four short sediment cores (BTP - Botany Point; REF - Refuge II; STH - Stenhouse; THP - Thomas Point) (red dots, Fig. 1 and Table 1) were collected during the

155 XXV Brazilian Antarctic Expedition (summer 2006/2007) using a mini-box corer (25 *
156 25 * 55 cm) (Ferreira et al., 2013; Martins et al. , 2010, 2014). The cores were generally
157 sectioned every 1 cm, and the samples were first stored at - 20 °C in previously calcined
158 aluminum trays. Samples for the analysis of radionuclides were stored in plastic
159 containers. Samples for the analysis of organic markers were freeze-dried, homogenized
160 in a mortar and stored in glass vials until laboratory analysis.
161
162 *3.2. Age Model*
163 The activity of radionuclide ^{137}Cs was determined by gamma spectrometry with
164 hyper-pure Germanium detector (model GEM60190, EGG & ORTEC) and the vertical
165 variation was used to estimate sedimentation rates. The detailed methods were first
166 published by Martins et al. (2010) and Ferreira et al. (2013) and the obtained
167 sedimentation rates are presented in Table 1.
168
169 *3.3. Total Organic Carbon (TOC)*
170 TOC analysis was conducted using 1.0 g of homogenized sediments. Samples
171 were pre-treated with hydrochloric acid, washed twice with deionized water to remove
172 chloride, and dried at 80 °C overnight. The TOC was determined using a Carlo Erba 1100
173 CHN Analyser with a precision of < ± 0.1 wt %. Measurements were performed in
174 duplicate and the average is reported here.
175
176 *3.4. Sample extraction, instrumental analysis and analytical control*
177 The analytical method used to extract the biomarkers (GDGTs, fatty alcohols and
178 sterols) consisted of ultrasonic extraction and alumina column fractionation. For this
179 purpose, dried sediments (ca. 10 - 15 g) were ultrasonically extracted with
180 dichloromethane (DCM; 2 times), DCM: methanol (MeOH) (1:1; v/v; 2 times) and
181 MeOH (2 times). The extracts were combined and evaporated to dryness and then
182 fractionated using solid phase extraction method and short alumina columns. The apolar
183 fraction was eluted with approximately 4.5 mL *n*-hexane: DCM (9:1, v/v), while the polar
184 fraction (containing the compounds of interest here) was eluted with approximately 6 mL
185 DCM:MeOH (1:2; v/v). The polar fraction was further divided into two portions, one for
186 the analysis of branched and isoprenoidal GDGTs and one for the analysis of fatty
187 alcohols and sterols. These extracts were dried under N_2 flow. The fraction for GDGT
188 analysis was resuspended in *n*-hexane: isopropanol (99: 1, v/v); filtered (PTFE filter, 0.45

μm); and concentrated to about 2 mg mL^{-1} prior to LC-MS analysis. The other portion destined for the analysis of fatty alcohols and sterols by GC-MS was derivatized using BSTFA and pyridine (heating at 70 °C for 1 h).

GDGTs were analyzed by high performance liquid chromatography coupled with atmospheric pressure chemical ionization mass spectrometry (HPLC-APCI-MS, Thermo Finnigan TSQ/Acela Series). All samples were measured in triplicate and the average values are reported here. Chromatographic separation of compounds was achieved using an Alltech Prevail Cyano column (2.1 mm i.d. × 150 mm, 3 μm). The GDGTs were eluted isocratically with *n*-hexane: isopropanol (99: 1, v/v) for 7 min, followed by a linear gradient to 1.3% isopropanol at 30 min, to 1.6% isopropanol at 35 min, then increasing to 10% isopropanol at 36 min and kept for 8 min (at a flow of 0.2 mL min^{-1}), finally equilibrating with 1% isopropanol for 13 min before the next injection. After each three analyses, the column was cleaned by back-flushing of *n*-hexane: isopropanol (99: 1, v/v) for 7 min and then rinsed by a linear gradient from 9: 1 (v/v) to 99: 1 (v/v) *n*-hexane: isopropanol within 14 min and equilibrated with 1% isopropanol at 30 min. The instrumental conditions for APCI-MS were: drying gas (N_2) flow 6 L min^{-1} and temperature 200 °C, vaporizer temperature of 380 °C, capillary temperature of 282 °C and corona discharge current of 3 μA. GDGTs were detected by APCI/MS in selected ion monitoring (SIM) mode (*m/z* 1302, 1300, 1298, 1296, 1292, 1050, 1048, 1046, 1036, 1034, 1032, 1022, 1020, 1018, 653 and 744). GDGTs were semi-quantified with an interval synthetic C_{46} tetraether standard.

The fatty alcohols and the sterols were analyzed by gas chromatography-mass spectrometry (GC-MS; ThermoQuest Trace GC interfaced to Finnigan Trace MS quadrupole spectrometer). Separation was achieved using a HP-1 fused silica capillary column (50 m × 0.32 mm i.d.; 0.17 μm film thickness). The injection was made at 70 °C and the temperature increased to 130 °C at 20 °C min^{-1}, then up to 300 °C at 4 °C min^{-1}, and then remained constant at 300 °C for 20 min. Helium was used as a carrier gas. The GC-MS operated in electron impact ionization (70 eV) and full scan mode (*m/z* 50-650). The internal standard to quantify the fatty alcohols and sterols was 2-hexadecane, added prior to GC-MS analysis. The analyte peak areas were integrated from the total ion current chromatograms.

221 *3.5. Data analysis*

222 The statistical analyses were performed in R version 3.5.1 (R Core Team, 2018)
223 using the packages Hmisc (Harrell Jr., 2019), pracma (Borchers, 2019) and WaveletComp
224 (Roesch and Schmidbauer, 2018), while the spatial analyses were performed using the
225 QGIS 3.4.2 software (QGIS Development Team, 2018).

226 First, we calculated four different indices to test if there are any potential sources
227 other than the planktonic Thaumarchaeota that could affect the GDGT-based
228 paleothermometry interpretation. The Branched and Isoprenoid Tetraether Index (BIT)
229 was proposed by Hopmans et al. (2004) to evaluate the relative input of terrestrial OM in
230 the marine environment.

231

232 BIT = ([brGDGT-I] + [brGDGT-II] + [brGDGT-III]) / ([crenarchaeol] + [brGDGT-I]
233 + [brGDGT-II] + [brGDGT-III])

234

235 The methane index (MI) was proposed by Zhang et al. (2011) to indicate the
236 relative contribution of GDGTs derived from methanotrophic Archaea to those from
237 planktonic Thaumarchaeota.

238

239 MI = ([isoGDGT-1] + [isoGDGT-2] + [isoGDGT-3]) / ([isoGDGT-1] + [isoGDGT-2]
240 + [isoGDGT-3] + [crenarchaeol] + [cren. isomer])

241

242 The ring index (RI) was proposed by Zhang et al. (2016) to indicate a potential
243 non-thermal influence on GDGTs distributions. |ΔRI| indicates the residual of a sample's
244 RI (RI_{sample}) from a calculated RI ($RI_{calculated}$) based on the global TEX_{86} − RI regression.

245

246 RI_{sample} = 0 * {isoGDGT-0} + 1 * {isoGDGT-1} + 2 * {isoGDGT-2} + 3 * {isoGDGT-
247 3} + 4 * {crenarchaeol} + 4 * {cren. isomer}

248

249 $RI_{calculated}$ = -0.77 (± 0.38) * TEX_{86} + 3.32 (± 0.34) * $(TEX_{86})^2$ + 1.59 (± 0.10)

250

251 $|\Delta RI| = RI_{calculated} - RI_{sample}$

252

253 Lastly, the % GDGT-0 was proposed by Sinninghe Damsté et al. (2012) to
254 indicate the contribution of methanogenic Archaea.

%GDGT-0 = [isoGDGT-0] / ([isoGDGT-0] + [crenarchaeol])

While the MI and %-GDGT-0 indices were calculated based on the compounds' abundance (brackets), the RI index was calculated based on the percentage of the compounds (braces).

The TEX_{86} index was calculated following Schouten et al. (2002):

TEX_{86} = ([isoGDGT-2] + [isoGDGT-3] + [cren. isomer]) / ([isoGDGT-1] + [isoGDGT-2] + [isoGDGT-3] + [cren. isomer])

In addition, we also calculated the TEX_{86}^{L} index (Kim et al., 2010):

$TEX_{86}^{L} = \log_{10}$ ([isoGDGT-2] / ([isoGDGT-1] + [isoGDGT-2] + [isoGDGT-3]))

To verify the applicability of the GDGT-based paleotemperature proxies to the polar environment, calculated temperatures based on the sediment cores GDGT data were compared with the interpolated mean temperature taken from the Simple Ocean Data Assimilation (SODA3) reanalysis data (Carton and Giese, 2008) (http://dsrs.atmos.umd.edu/DATA/soda3.3.2). The data are initially based on a numerical model and then corrected based on direct observations. They have a final horizontal resolution of 0.25° * 0.25° and cover the period between 1980 and 2015 (Carton et al., 2018). The GDGT-based temperatures were compared with the annual mean and seasonal temperatures (from 1980 to 2006) corresponding to the nearest interpolated 0.50º gridbox (average of the surrounding four grid cells). To explore the influence of seasonality, we calculate quarterly averages, using different combinations of months. For example, the "summer 1" season was formed by the December, January and February months (the usual combination); the "summer 2" combination was formed by January, February and March; and the "summer 3" combination was formed by February, March and April. Finally, the fit between GDGT-based SST and satellite-based SST was tested using the Spearman correlation test because not all datasets were normally distributed. The five GDGT-based SST calibrations we tested here were proposed by Kim et al. (2010), Shevenell et al. (2011), Tierney and Tingley (2014), Park et al. (2019), and Dunkley Jones et al. (2020).

All plots from the Bellingshausen Station (see Fig. 1) are based on data from the Antarctic Research and Investigation subprogram, obtained from the READER (Reference Antarctic Data for Environmental Research), a project of the Scientific Committee on Antarctic Research (AARI, 2019). The precipitation data are presented as monthly sums (in mm), while the wind speeds are presented as monthly means (in m^{-1}).

4. Results

4.1. OM input

The BTP is the longest sediment core with the highest temporal resolution. Therefore, we analyzed the OM variation and its dependence on SST and other environmental parameters using this record only. In this core that spans the last 50 years, there is a similar trend in concentration for the sterols, alcohols, and isoGDGTs and this trend is also similar to that seen in the TOC record (Fig. 2). At first (~ 1963 to 1975), the concentrations decreased, followed by a gradual increase between 1975 and 1998. The input slightly decreased after 2000.

The dominant sterols were cholest-5-en-3β-ol (cholesterol; $27\Delta^5$) and 24-ethylcholest-5-en-3β-ol (sitosterol; $29\Delta^5$). (Fig. 3). The 5α-stanols were less abundant than their unsaturated analogues, being normally diagenetically produced by the microbial reduction of Δ^5-stenols into 5α-stanols (Grimalt et al., 1990). The ratio 5α-stanols/Δ^5-stenols was generally higher than 0.5. Other abundant compounds were the *n*-alkanol *n*-C_{16}-OH and phytol. All sediments contained isoGDGTs. The main GDGTs found in our sampling site were GDGT-0 and crenarchaeol, representing around 50% and 40% of the isoGDGT distribution, respectively.

4.2. IsoGDGTs and calibration of the SST estimates

Various indices have been proposed to characterize the source of sedimentary isoGDGTs (and, by extension, their suitability for SST reconstruction). GDGTs can be derived from terrestrial sources or be produced in the water column and/or within sediments (Sinninghe Damsté et al., 2012; Schouten et al., 2013; Zhang et al., 2016). The Branched and Isoprenoid Tetraether Index (BIT) indicates the terrestrial input of GDGTs to marine sediments when it exceeds 0.3 (Hopmans et al., 2004; Weijers et al., 2006). Overall, the BIT varied between 0.04 and 0.07 at BTP sediment core (Supplementary

Table S1), suggesting that effect of the fluvial input of terrestrially derived isoprenoid GDGTs on the GDGT-based paleothermometry may be negligible.

The methane index (MI) indicates the relative contribution of GDGTs derived from methanotrophic Archaea (Zhang et al., 2011), when its values exceed 0.3. The MI in our samples was low with a maximum of 0.07 (Supplementary Table S1). Similarly, the % GDGT-0 indicates the contribution of methanogenic Archaea when it exceeds 67% (Sinninghe Damsté et al., 2012). These varied between 44 and 88% across the four cores. For the BTP, REF and THP cores all sediments had values < 67%. The STH core had 6 samples between 4.5 and 12.5 cm deep (spanning the years 1977-1994), with a % GDGT-0 > 67% (Supplementary Table S1).

The ring index residual (|ΔRI|) is less clearly linked to specific biological sources but is indicates a non-temperature influence on GDGT distributions when it exceeds 0.3 (Zhang et al., 2016). The |ΔRI| varied between 0.03 and 1.53. In the BTP, TEF and THP cores most samples had a |ΔRI| value < 0.3. Sediments from the STH core, those between 4.5 and 12.5 cm deep (spanning the years 1977-1994), all had values > 0.3 with maxima > 1 (Supplementary Table S1). Therefore, the BIT, MI, |ΔRI|, and % isoGDGT-0 all indicate that the majority of isoGDGTs are produced within the water column. For the STH core, the indices suggest a contribution of archaeal groups other than the planktonic Thaumarchaeota to the isoGDGT pool.

We then determined the temperature estimates using five GDGT-based calibrations. These are the TEX_{86}^{L} calibration proposed by Kim et al. (2010) for (sub)polar oceans, the TEX_{86} calibration developed by Shevenell et al. (2011) for the Antarctic Peninsula, the global BAYSPAR TEX_{86} calibration (using the surface mode) of Tierney and Tingley (2014) that is based on a spatially-varying calibration model, the TEX_{86}^{L} calibration by Park et al. (2019) using a polynomial calibration for the Southern Ocean, and the OPTiMAL calibration proposed by Dunkley Jones et al. (2020) based on the distribution of six isoprenoid GDGTs. These temperatures can be compared to those obtained from the SODA reanalysis, considering the annual and seasonal means. Samples with MI, |ΔRI|, and % isoGDGT-0 values above the thresholds were excluded from this analysis. The only quarterly combination that presented significant correlation values (p-value < 0.05) was: JFM = austral summer, AMJ = austral autumn, JAS = austral winter, OND = austral spring (Supplementary Table S2). The Spearman correlation analysis indicated that the best fit was achieved with the austral spring season (Oct-Nov-Dec) (Table 2).

Based on these results, we compared the SODA-based SST from the austral spring season (OND) with the temperature estimates obtained with the five calibration methods (Fig. 4). Using this approach, the AntPen calibration proposed by Shevenell et al. (2011) significantly overestimated the SST at all three locations. The OPTiMAL calibration by Dunkley Jones et al. (2020) also overestimated the SST at all three locations, whereas the TEX_{86}^{L} and BAYSPAR calibrations proposed by Kim et al. (2010) and Tierney and Tingley (2014), respectively, overestimated the SST only when the TEX_{86} values exceeded 0.45. The quadratic calibration proposed by Park et al. (2019) provides the best fit with the reanalysis record.

5. Discussion

5.1. OM input and temporal evolution

As observed in Fig. 2, the OM proxies did not exhibit homogenous behaviors during the last 50 years. The differences among the biomarker records may have been caused by changes in the productivity of the source organisms. Thus, we first explored the source of the OM proxies before discussing their temporal evolution.

The most abundant sterol is the cholest-5-en-3β-ol. It can be produced by phytoplankton and zooplankton, and is present in the feces of penguins and pinnipeds (Wisnieski et al., 2014). The similarity between the profiles of cholest-5-en-3β-ol and 24-methylcholest-5,22E-dien-3β-ol (brassicasterol; $28\Delta^{5,22}$; a marker for diatoms – Volkman, 1986) corroborates phyto- and zooplankton as the main sources for cholest-5-en-3β-ol (Fig. 3). The only exception is the sample around the year 2004, when the peak of cholest-5-en-3β-ol does not coincide with an increase in the methylcholest-5,22E-dien-3β-ol input. During this period, cholest-5-en-3β-ol probably had a significant contribution from penguin feces, since the regions of Ulmann Point and Keller Peninsula are used for penguins to molt their feathers (Weber and Montone, 2006). The second most abundant sterol is the 24-ethylcholest-5-en-3β-ol (sitosterol; $29\Delta^{5}$) (Fig. 3). This sterol predominance was also found by Wisnieski et al. (2014) in Admiralty Bay, and they attributed the 24-ethylcholest-5-en-3β-ol to macro- and microalgae. The similarity between the profiles of 24-ethylcholest-5-en-3β-ol and 24-methylcholest-5,22E-dien-3β-ol corroborates the diatoms as the probable main source for the 24-ethylcholest-5-en-3β-ol.

The main fatty alcohols are the *n*-alkanol *n*-C_{16}-OH and phytol (Fig. 3). The *n*-alkanol *n*-C_{16}-OH s usually associated with aquatic algae, bacteria and zooplankton (Wisnieski et al., 2014). However, the absence of similarity between the *n*-alkanol *n*-C_{16}-OH, cholest-5-en-3β-ol, 24-methylcholest-5,22E-dien-3β-ol and phytol suggests that this short-chain *n*-alkanol is neither derived from aquatic algae nor zooplankton, but probably from non-photosynthetic organisms, such as bacteria. Phytol (3,7,11,15-tetramethyl-2-hexadecen-1-ol), on the other hand, has been used as a marker of photosynthetic organisms since it is derived from the degradation of chlorophyll-*a* (Volkman et al., 2008). Its depth profile is similar to that of 24-methylcholest-5,22E-dien-3β-ol, suggesting similar sources. However, high phytol concentrations between 1980 and 1985 are not accompanied by changes in the concentrations of other microalgae biomarkers (24-methylcholest-5,22E-dien-3β-ol, 24-ethylcholest-5-en-3β-ol and 4α,23,24-trimethylcholesta-22E-en-3β-ol – dinosterol, $30\Delta^{22}$). This suggests an input from other photosynthetic producers, such as cyanobacteria or macroalgae.

Finally, as observed in Fig. 3, the ratio of 5α-stanols/Δ^5-stenols was generally higher than 0.5, suggesting significant alteration of the sedimentary OM due to bacterial activity (Wakeham and Canuel, 2006; Wisnieski et al., 2014). The values of the ratio $29\Delta^0/29\Delta^5$ decreased from the bottom to the top of the sediment core, indicating a strong diagenetic activity after the final burial of OM in the sediment. The values of the ratio $27\Delta^0/27\Delta^5$, on the other hand, presented higher values around 1970 and after 1990. Since the cholest-5-en-3β-ol ($27\Delta^5$) and the 24-ethylcholest-5-en-3β-ol ($29\Delta^5$) have distinct sources, the difference between the 5α-stanols/Δ^5-stenols profiles may indicate a preferential degradation between different organic compounds.

Regardless of source, most compounds (24-methylcholest-5,22E-dien-3β-ol, 24-ethylcholest-5-en-3β-ol, 4α,23,24-trimethylcholesta-22E-en-3β-ol and phytol profiles in Fig. 4) indicate elevated phytoplankton productivity between 1963 and 1975, and between 2000 and 2006.

Between 2002 and 2009, Lange et al. (2015) also found significantly higher phytoplankton abundances in Botany Point compared to the region in front of Keller Peninsula. Among several parameters, they found that precipitation showed the largest influence over phytoplankton populations, with the most productive years coincident with high precipitation in summer. According to Nędzarek (2008), the main nutrient sources to the Admiralty Bay are the continental runoff of freshwater enriched in biogenic compounds from the penguin rookeries, and the decomposition of macroalgae. Thus, high

421 precipitation rates can increase the continental runoff, increasing nutrient supply to the
422 coastal region. Lange et al. (2015) also observed a negative correlation between the wind
423 speed and the phytoplankton abundance. Strong winds tend to increase the water
424 turbidity, decreasing light penetration and primary production (Pichlmaier et al., 2004;
425 Lange et al., 2015). The first precipitation and wind speed data for the King George Island
426 were obtained at the Bellingshausen research station in 1968 (Fig. 5) (SCAR Reader
427 Project, 2019). Based on the available data, the relatively low wind speed coupled to high
428 precipitation in the late 1960s may have been responsible for the high marine productivity
429 in the beginning of the record and its decreasing trend towards 1975 (Fig. 5).
430 Between 1976 and 1998, increase in algal biomarker abundances could have been
431 caused by a slightly wetter and warming weather (Kejna et al., 2013). However, the large
432 input of alcohols and isoprenoid GDGTs between 1980 and 1987 does not correspond to
433 any of these parameters (precipitation in Fig. 5 and SST and Fig. 6). A possible
434 explanation is glacier retraction. Between 1979 and 1988, Rosa et al. (2014) reported high
435 area loss of the main glaciers around the BTP sampling site, especially the Krak glacier
436 (Fig. 5, rightmost panel). The melted water may have carried continental nutrients to the
437 coastal region.
438 After that, there was a relative stabilization in the OM input. The largest variation
439 occurred in 2004, where the increase in sterol concentration was driven mainly by a peak
440 in the cholest-5-en-3β-ol concentrations. As discussed above, since this increase was not
441 accompanied by a proportional increase in the phytoplankton biomarkers, it is more
442 plausible that it is derived from penguin feces, instead of from the zooplankton. It
443 suggests an increase in the population of ice-tolerant penguin species, such as gentoo
444 penguins (Henley et al., 2019), around Botany Point. That may have been caused by the
445 retreat of the glaciers, exposing ice-free land areas (Oliveira et al., 2019). This increase
446 in the supply of ornithogenic nutrients, in turn, may have promoted the marine
447 productivity.
448
449 *5.2. IsoGDGTs and calibration of the SST estimates*
450 As mentioned earlier, some caution should be taken before applying the GDGT-
451 based indices to reconstruct temperature because of the possibility of alternative sources
452 for the isoGDGTs other than planktonic Thaumarchaeota. When applied to the STH
453 record, the RI indicated a potential non-thermal influence between 1977 and 1996, while

454 a potential contribution from methanogens was observed between 1984 and 1994
455 (Supplementary Table S1).
456 After discounting source effects, we found a strong positive correlation between
457 GDGT-based SST and austral spring SST (Oct-Nov-Dec; Table 2). Only the calibration
458 proposed by Dunkley Jones et al. (2020) did not exhibit a positive correlation with the
459 annual or any of the seasonal means. In 2011, Nakayama et al. found that the archaeal
460 communities in Martel Inlet are dominated by the phylum Thaumarchaeota (formerly
461 known as Crenarchaeota), a major source of the isoprenoid GDGTs used in the TEX_{86}
462 calculation (Schouten et al., 2002, 2013). In 2015, Hernández et al. studied the marine
463 archaeal community structure in Potter Cove, a shallow water coastal marine area located
464 in the King George Island. They also observed a high dominance of members of the
465 phylum Thaumarchaeota, specially during the spring. During this season, the increase in
466 solar radiation and temperature promotes primary productivity. The warmer temperatures
467 also increase freshwater run-off, delivering more suspended particulate matter (SPM) to
468 the water column. The higher primary productivity rates coupled with the SPM input
469 enhances the growth of Thaumarchaeota. More recently, Signori et al. (2018) studied the
470 seasonal changes in bacterial and archaeal diversity and community structure in the
471 Bransfield Strait. Their results indicate that seasonal variation of temperature and OM
472 production are regulatory factors affecting the bacterial and archaeal communities.
473 During spring, the phylum Thaumarchaeota represents an important fraction (more than
474 5%) of the microbial community. However, in the summer, its relative abundance drops
475 to 1% or less, being outcompeted by bacteria. These microbial community dynamics
476 likely explain the high correlation between the GDGT-based SSTs and the austral spring
477 season SST.
478 Of five calibrations tested, that proposed by Park et al. (2019) presented the best
479 fit to SODA-based SST from the austral spring season (OND) (Fig. 4). However, because
480 it is a quadratic calibration, it could generate ambiguous values. The inflection of the
481 calibration curve is around 7 °C and historical SST means do not exceed 2 °C (neither
482 when analysing annual means nor spring means) (Supplementary Fig. S1). Thus, we
483 assume that only the cold temperature estimates are accurate and used the calibration
484 proposed by Park et al. (2019) in the subsequent analysis.
485

5.3. SST trends

Using the calibration proposed by Park et al. (2019), we calculated SST for the sediment core at BTP, since it is the longest one with the highest temporal resolution. The TEX_{86}-based temperatures from BTP, considering the calibration errors, are in the same range as the mean air temperatures observed in the King George Island by Kejna et al. (2013) (Fig. 6, top panel). The period between 1979 and 2000 had the largest observed glacier retreat in the Martel Inlet (Rosa et al., 2014). This warming trend is observed in the TEX_{86}-based SST records. After 1998, however, we detect no warming in the BTP record (Fig. 6, bottom panel), similar to observations of the Antarctic Peninsula by Turner et al. (2016) and Huai et al. (2019). Low SST values were observed around 1977, 1996 and 2004. They did not coincide with consistent patterns of decreased freshwater input, through either precipitation or meltwater inflow from the adjacent glaciers. However, these cooler periods coincided with relatively high wind speed values that may have promoted the water column mixture bringing colder waters to the surface (Fig. 5).

Finally, changes in the OM production did not affect the SST reconstruction. Hurley et al. (2018) found that the sedimentary TEX_{86} values may under-predict local SST in regions of high productivity. After blooming episodes, common in polar environments, ammonia released by remineralization of organic matter may promote archaeal ammonia oxidation rate and growth rate. However, the correlations between SST values and the organic matter proxies in this study were low ($|R_s| < 0.17$) and non-significant (p-value < 0.05) (Supplementary Table S3). While the largest variations in the OM were observed mainly between 1965 and 1980, the largest SST variation occurred around the year 2000 (Fig. 5).

6. Conclusions

We evaluated the performance of the TEX_{86} proxy in four short sedimentary cores collected in the Admiralty Bay, King George Island, that span the second half of the 20th century; we complemented that investigation with analyses of OM sources in the longest and most complete of these cores.

Combined with meteorological data, we were able to examine causes in dramatic and unexpected variations in primary productivity. Before 1975, the primary productivity was primarily driven by precipitation and wind dynamics. An increase in phytoplankton productivity occurred between 1985 and 2000, probably promoted by SST warming and

519 the relatively wetter climate. Glacier retreats near the sampling site may also have
520 promoted the primary productivity, especially in the early 1980s and late 1990s. In the
521 last part of the record, there was a relative stabilization in the OM input coupled with a
522 cooling SST trend. The exception was around the year 2004, when a peak of cholesterol
523 decoupled from environmental proxies and other biomarkers likely documents an
524 increase in the contribution from "ice-tolerant" penguins.
525 As there are still no studies on the reconstruction of SST variations in the region,
526 we tested five different calibrations developed for the Antarctic environment. The
527 comparison between GDGT-based SST estimates (using five calibrations) and reanalysis-
528 based SST (annual and seasonal means) indicated that the GDGT signal represents the
529 austral spring season (Oct/Nov/Dec). The calibration that provided the best fit with the
530 reanalysis-based SST was the quadratic calibration proposed by Park et al. (2019).
531 Variations in OM production did not present any significant effect on the GDGT-based
532 paleothermometry. This confirms the potential utility of GDGT-based SST proxies in this
533 region and allowed us to develop a SST record from 1960 to 2010.
534

535 **Acknowledgements**

536 The work was supported by the Antarctic Brazilian Program (PROANTAR), Secretaria
537 da Comissão Interministerial para os Recursos do Mar (SECIRM), Conselho Nacional de
538 Desenvolvimento Científico e Tecnológico (CNPq, 550014/2007-1 and 442692/2018-8)
539 and Coordenação de Aperfeiçoamento de Pessoal de Ensino Superior (CAPES,
540 88887.314458/2019-00). The authors wish to thank the 'Comandante Ferraz' Brazilian
541 Antarctic Station staff for support during the sampling activities. B.D.A. Naafs
542 acknowledges funding through a Royal Society Tata University Research Fellowship.
543 NERC (Reference: CC010) and NEIF (www.isotopesuk.org) are thanked for funding and
544 maintenance of the GC-MS and LC-MS instrument at the University of Bristol used for
545 this work. C.C. Martins and A.L.L. Dauner thanks CAPES by personal grants support
546 (BEX 5366/12-7 and 88887.362846/2019-00, respectively). Finally, this work is part of
547 CARBMET project (The multiple faces of organic CARBon and METals in the sub-
548 Antarctic ecosystem) sponsored by CNPq, CAPES and Brazilian Ministry of Science,
549 Technology, Innovation and Communication.

References

AARI, 2019. Antarctic Research and Investigation (http://www.aari.aq/default_en.html) [WWW Document]. URL http://www.aari.aq/default_en.html (accessed 10.24.19).

Berbel, G.B.B., Braga, E.S., 2014. Phosphorus in Antarctic surface marine sediments - Chemical speciation in Admiralty Bay. Antarctic Science 26, 281–289.

Borchers, H.W., 2019. pracma: Practical Numerical Math Functions, v.2.2.5.

Brandini, F.P., Rebello, J., 1994. Wind field effect on hydrography and chlorophyll dynamics in the coastal pelagial of Admiralty Bay, King George Island, Antarctica. Antarctic Science 6, 433–442.

Braun, M.H., Saurer, H., Goßmann, H., 2004. Climate, energy fluxes and ablation rates on the ice cap of King George Island. Pesquisa Antártica Brasileira 103, 87–103.

Braun, M.H., Saurer, H., Vogt, S., Simões, J.C., Goßmann, H., 2001. The influence of large-scale atmospheric circulation on the surface energy balance of the King George Island ice cap. International Journal of Climatology 21, 21–36.

Carton, J.A., Chepurin, G.A., Chen, L., 2018. SODA3: A new ocean climate reanalysis. Journal of Climate 31, 6967–6983.

Carton, J.A., Giese, B.S., 2008. A reanalysis of ocean climate using Simple Ocean Data Assimilation (SODA). Monthly Weather Review 136, 2999–3017.

Ceschim, L.M.M., Dauner, A.L.L., Montone, R.C., Figueira, R.C.L., Martins, C.C., 2016. Depositional history of sedimentary sterols around Penguin Island, Antarctica. Antarctic Science 28, 443–454.

De Rosa, M., Esposito, E., Gambacorta, A., Nicolaus, B., Bu'Lock, J.D., 1980. Effects of temperature on ether lipid composition of Caldariella acidophila. Phytochemistry 19, 827–831.

Dunkley Jones, T., Eley, Y., Thomson, W., Greene, S.E., Mandel, I., Edgar, K.M., Bendle, J., 2020. OPTiMAL: a new machine learning approach for GDGT-based palaeothermometry. Climate of the Past 16, 2599–2617.

Eglinton, T.I., Eglinton, G., 2008. Molecular proxies for paleoclimatology. Earth and Planetary Science Letters 275, 1–16.

Elling, F.J., Könneke, M., Mußmann, M., Greve, A., Hinrichs, K.U., 2015. Influence of temperature, pH, and salinity on membrane lipid composition and TEX86 of marine planktonic thaumarchaeal isolates. Geochimica et Cosmochimica Acta 171, 238–255.

Etourneau, J., Collins, L.G., Willmott, V., Kim, J.H., Barbara, L., Leventer, A.,

584 Schouten, S., Sinninghe Damsté, J.S., Bianchini, A., Klein, V., Crosta, X., Massé,
585 G., 2013. Holocene climate variations in the western Antarctic Peninsula: Evidence
586 for sea ice extent predominantly controlled by changes in insolation and ENSO
587 variability. Climate of the Past 9, 1431–1446.
588 Fávaro, D.I.T., Silva, P.S.C., Mazzilli, B.P., Cavallaro, G.P.M., Taddei, M.H.T., Berbel,
589 G.B.B., Braga, E.S., 2011. Sediment geochemistry in Admiralty Bay (Antarctica):
590 trace, rare earth elements and radionuclides. Brazilian Antarctic Research 5, 1–14.
591 Ferreira, P.A.L., Ribeiro, A.P., Nascimento, M.G., Martins, C.C., Mahiques, M.M.,
592 Montone, R.C., Figueira, R.C.L., 2013. 137Cs in marine sediments of Admiralty
593 Bay, King George Island, Antarctica. Science of the Total Environment 443, 505–
594 510.
595 Fietz, S., Ho, S.L., Huguet, C., Rosell-Melé, A., Martínez-García, A., 2016. Appraising
596 GDGT-based seawater temperature indices in the Southern Ocean. Organic
597 Geochemistry 102, 93–105.
598 Grimalt, J.O., Fernandez, P., Bayona, J.M., Albaigés, J., 1990. Assessment of fecal
599 sterols and ketones as indicators of urban sewage inputs to coastal waters.
600 Environmental Science & Technology 24, 357–363.
601 Harrell Jr., F.E., 2019. Hmisc: Harrell Miscellaneous, v. 4.1.1.
602 Henley, S.F., Schofield, O.M., Hendry, K.R., Schloss, I.R., Steinberg, D.K., Moffat, C.,
603 Peck, L.S., Costa, D.P., Bakker, D.C.E., Hughes, C., Rozema, P.D., Ducklow,
604 H.W., Abele, D., Stefels, J., Van Leeuwe, M.A., Brussaard, C.P.D., Buma, A.G.J.,
605 Kohut, J., Sahade, R., Friedlaender, A.S., Stammerjohn, S.E., Venables, H.J.,
606 Meredith, M.P., 2019. Variability and change in the west Antarctic Peninsula
607 marine system: Research priorities and opportunities. Progress in Oceanography
608 173, 208–237.
609 Hernández, E.A., Piquet, A.M.T., Lopez, J.L., Buma, A.G.J., MacCormack, W.P., 2015.
610 Marine archaeal community structure from Potter Cove, Antarctica: high temporal
611 and spatial dominance of the phylum Thaumarchaeota. Polar Biology 38, 117–130.
612 Hertzberg, J.E., Schmidt, M.W., Bianchi, T.S., Smith, R.K., Shields, M.R.,
613 Marcantonio, F., 2016. Comparison of eastern tropical Pacific TEX86 and
614 Globigerinoides ruber Mg/Ca derived sea surface temperatures: Insights from the
615 Holocene and Last Glacial Maximum. Earth and Planetary Science Letters 434,
616 320–332.
617 Ho, S.L., Mollenhauer, G., Fietz, S., Martínez-García, A., Lamy, F., Rueda, G.,

618 Schipper, K., Méheust, M., Rosell-Melé, A., Stein, R., Tiedemann, R., 2014.
619 Appraisal of TEX86 and TEX86L thermometries in subpolar and polar regions.
620 Geochimica et Cosmochimica Acta 131, 213–226.
621 Hopmans, E.C., Weijers, J.W.H., Schefuß, E., Herfort, L., Sinninghe Damsté, J.S.,
622 Schouten, S., 2004. A novel proxy for terrestrial organic matter in sediments based
623 on branched and isoprenoid tetraether lipids. Earth and Planetary Science Letters
624 224, 107–116.
625 Huai, B., Wang, Y., Ding, M., Zhang, J., Dong, X., 2019. An assessment of recent
626 global atmospheric reanalyses for Antarctic near surface air temperature.
627 Atmospheric Research 226, 181–191.
628 Huang, J., Sun, L., Wang, X., Wang, Y., Huang, T., 2011. Ecosystem evolution of seal
629 colony and the influencing factors in the 20th century on Fildes Peninsula, West
630 Antarctica. Journal of Environmental Sciences 23, 1431–1436.
631 Hurley, S.J., Lipp, J.S., Close, H.G., Hinrichs, K.U., Pearson, A., 2018. Distribution and
632 export of isoprenoid tetraether lipids in suspended particulate matter from the
633 water column of the Western Atlantic Ocean. Organic Geochemistry 116, 90–102.
634 Jaeschke, A., Wengler, M., Hefter, J., Ronge, T.A., Geibert, W., Mollenhauer, G.,
635 Gersonde, R., Lamy, F., 2017. A biomarker perspective on dust, productivity, and
636 sea surface temperature in the Pacific sector of the Southern Ocean. Geochimica et
637 Cosmochimica Acta 204, 120–139.
638 Kaur, G., Mountain, B.W., Stott, M.B., Hopmans, E.C., Pancost, R.D., 2015.
639 Temperature and pH control on lipid composition of silica sinters from diverse hot
640 springs in the Taupo Volcanic Zone, New Zealand. Extremophiles 19, 327–344.
641 Kejna, M., Araźny, A., Sobota, I., 2013. Climatic change on King George Island in the
642 years 1948 – 2011. Polish Polar Research 34, 213–235.
643 Kim, J.H., van der Meer, J., Schouten, S., Helmke, P., Willmott, V., Sangiorgi, F., Koç,
644 N., Hopmans, E.C., Sinninghe Damsté, J.S., 2010. New indices and calibrations
645 derived from the distribution of crenarchaeal isoprenoid tetraether lipids:
646 Implications for past sea surface temperature reconstructions. Geochimica et
647 Cosmochimica Acta 74, 4639–4654.
648 Lange, P.K., Tenenbaum, D.R., Tavano, V.M., Paranhos, R., Campos, L.S., 2015. Shifts
649 in microphytoplankton species and cell size at Admiralty Bay, Antarctica.
650 Antarctic Science 27, 225–239.
651 Machado, A., Chemale Jr., F., Lima, E.F., Figueiredo, A.M.G., 1998. Petrologia das

652 rochas vulcânicas da Península Fildes, Ilha Rei George, Antártica. Pesquisas em
653 Geociências 25, 35–42.
654 Machado, A., Lima, E.F., Chemale Jr., F., Liz, J.D., Ávila, J.N., 2001. Química mineral
655 das rochas vulcânicas da Península Fildes (Ilha Rei George), Antártica. Revista
656 Brasileira de Geociências 31, 299–306.
657 Martins, C.C., Aguiar, S.N., Wisnieski, E., Ceschim, L.M.M., Figueira, R.C.L.,
658 Montone, R.C., 2014. Baseline concentrations of faecal sterols and assessment of
659 sewage input into different inlets of Admiralty Bay, King George Island,
660 Antarctica. Marine Pollution Bulletin 78, 218–23.
661 Martins, C.C., Bícego, M.C., Rose, N.L., Taniguchi, S., Lourenço, R.A., Figueira,
662 R.C.L., Mahiques, M.M., Montone, R.C., 2010. Historical record of polycyclic
663 aromatic hydrocarbons (PAHs) and spheroidal carbonaceous particles (SCPs) in
664 marine sediment cores from Admiralty Bay, King George Island, Antarctica.
665 Environmental Pollution 158, 192–200.
666 Martins, C.C., Montone, R.C., Gamba, R.C., Pellizari, V.H., 2005. Sterols and fecal
667 indicator microorganisms in sediments from Admiralty Bay, Antarctica. Brazilian
668 Journal of Oceanography 53, 1–12.
669 Nakayama, C.R., Kuhn, E., Araújo, A.C. V., Alvalá, P.C., Ferreira, W.J., Vazoller, R.F.,
670 Pellizari, V.H., 2011. Revealing archaeal diversity patterns and methane fluxes in
671 Admiralty Bay, King George Island, and their association to Brazilian Antarctic
672 Station activities. Deep-Sea Research Part II: Topical Studies in Oceanography 58,
673 128–138.
674 Nędzarek, A., 2008. Sources, diversity and circulation of biogenic compounds in
675 Admiralty Bay, King George Island, Antarctica. Antarctic Science 20, 135–145.
676 Oliveira, M.A.G. de, Rosa, K.K., Vieira, R., Simões, J.C., 2019. Variação de área das
677 geleiras do campo de gelo Kraków, Ilha Rei George, Antártica, no período entre
678 1956-2017. Revista Caminhos de Geografia 20, 55–71.
679 Park, E., Hefter, J., Fischer, G., Hvitfeldt Iversen, M., Ramondenc, S., Nöthig, E.M.,
680 Mollenhauer, G., 2019. Seasonality of archaeal lipid flux and GDGT-based
681 thermometry in sinking particles of high-latitude oceans: Fram Strait (79°N) and
682 Antarctic Polar Front (50°S). Biogeosciences 16, 2247–2268.
683 Park, E., Hefter, J., Fischer, G., Mollenhauer, G., 2018. TEX86 in sinking particles in
684 three eastern Atlantic upwelling regimes. Organic Geochemistry 124, 151–163.
685 Pearson, A., Huang, Z., Ingalls, A.E., Romanek, C.S., Wiegel, J., Freeman, K.H.,

686 Smittenberg, R.H., Zhang, C.L., 2004. Nonmarine crenarchaeol in Nevada hot
687 springs. Applied and Environmental Microbiology 70, 5229–5237.
688 Petrick, B.F., McClymont, E.L., Littler, K., Rosell-Melé, A., Clarkson, M.O., Maslin,
689 M., Röhl, U., Shevenell, A.E., Pancost, R.D., 2018. Oceanographic and climatic
690 evolution of the southeastern subtropical Atlantic over the last 3.5 Ma. Earth and
691 Planetary Science Letters 492, 12–21.
692 Pichlmaier, M., Aquino, F.E., Silva, C.S. da, Braun, M.H., 2004. Suspended sediments
693 in Admiralty Bay, King George Island (Antarctica). Pesquisa Antártica Brasileira
694 85, 77–85.
695 QGIS Development Team, 2018. QGIS Geographic Information System. Open Source
696 Geospatial Foundation Project.
697 R Core Team, 2018. R: A language and environment for statistical computing.
698 Rakusa-Suszczewski, S., 1995. The hydrography of Admiralty Bay and its inlets, coves
699 and lagoons (King George Island, Antarctica). Polish Polar Research 16, 61–70.
700 Robakiewicz, M., Rakusa-Suszczewski, S., 1999. Application of 3D circulation model
701 to Admiralty Bay, King George Island, Antarctica. Polish Polar Research 20, 43–
702 58.
703 Robinson, S.A., Ruhl, M., Astley, D.L., Naafs, B.D.A., Farnsworth, A.J., Bown, P.R.,
704 Jenkyns, H.C., Lunt, D.J., O'Brien, C., Pancost, R.D., Markwick, P.J., 2017. Early
705 Jurassic North Atlantic sea-surface temperatures from TEX86 palaeothermometry.
706 Sedimentology 64, 215–230.
707 Roesch, A., Schmidbauer, H., 2018. WaveletComp: Computational Wavelet Analysis,
708 v. 1.1.
709 Rosa, K.K., Freiberger, V.L., Vieira, R., Rosa, C.A., Simões, J.C., 2014. Glacial recent
710 changes and climate variability in King George Island, Antarctica. Quaternary and
711 Environmental Geosciences 05, 176–183.
712 Rückamp, M., Braun, M.H., Suckro, S., Blindow, N., 2011. Observed glacial changes
713 on the King George Island ice cap, Antarctica, in the last decade. Global and
714 Planetary Change 79, 99–109.
715 SCAR Reader Project, 2019. Surface meteorology at British Antarctic Survey Stations,
716 1947-2013 [WWW Document]. URL https://legacy.bas.ac.uk/met/READER/
717 (accessed 10.24.19).
718 Schouten, S., Hopmans, E.C., Schefuß, E., Sinninghe Damsté, J.S., 2002. Distributional
719 variations in marine crenarchaeol membrane lipids: a new tool for reconstructing

ancient sea water temperatures? Earth and Planetary Science Letters 204, 265–274.
Schouten, S., Hopmans, E.C., Sinninghe Damsté, J.S., 2013. The organic geochemistry of glycerol dialkyl glycerol tetraether lipids: A review. Organic Geochemistry 54, 19–61.
Shetye, S., Jena, B., Mohan, R., 2017. Dynamics of sea-ice biogeochemistry in the coastal Antarctica during transition from summer to winter. Geoscience Frontiers 8, 507–516.
Shevenell, A.E., Ingalls, A.E., Domack, E.W., Kelly, C., 2011. Holocene Southern Ocean surface temperature variability west of the Antarctic Peninsula. Nature 470, 250–254.
Signori, C.N., Pellizari, V.H., Enrich-Prast, A., Sievert, S.M., 2018. Spatiotemporal dynamics of marine bacterial and archaeal communities in surface waters off the northern Antarctic Peninsula. Deep-Sea Research Part II: Topical Studies in Oceanography 149, 150–160.
Simões, J.C., Bremer, U.F., Aquino, F.E., Ferron, F.A., 1999. Morphology and variations of glacial drainage basins in the King George Island ice field, Antarctica. Annals of Glaciology 29, 220–224.
Sinninghe Damsté, J.S., Ossebaar, J., Schouten, S., Verschuren, D., 2012. Distribution of tetraether lipids in the 25-ka sedimentary record of Lake Challa: extracting reliable TEX86 and MBT/CBT palaeotemperatures from an equatorial African lake. Quaternary Science Reviews 50, 43–54.
Smellie, J.L., Pankhurst, R.J., Thomson, M.R.A., Davies, R.E.S., 1984. The geology of the South Shetland Islands: VI. Stratigraphy, geochemistry and evolution., in: British Antarctic Survey Scientific Reports. Cambridge, p. 85.
Tierney, J.E., Tingley, M.P., 2014. A Bayesian, spatially-varying calibration model for the TEX86 proxy. Geochimica et Cosmochimica Acta 127, 83–106.
Turner, J., Lu, H., White, I., King, J.C., Phillips, T., Hosking, J.S., Bracegirdle, T.J., Marshall, G.J., Mulvaney, R., Deb, P., 2016. Absence of 21st century warming on Antarctic Peninsula consistent with natural variability. Nature 535, 411–415.
Volkman, J.K., 1986. A review of sterol markers for marine and terrigenous organic matter. Organic Geochemistry 9, 83–99.
Volkman, J.K., 2006. Lipid markers for marine organic matter, in: Volkman, J.K. (Ed.), Marine Organic Matter: Biomarkers, Isotopes and DNA. The Handbook of Environmental Chemistry, Vol 2N. Springer, Berlin, Heidelberg, pp. 27–70.

754 Volkman, J.K., Revill, A.T., Holdsworth, D.G., Fredericks, D., 2008. Organic matter
755 sources in an enclosed coastal inlet assessed using lipid biomarkers and stable
756 isotopes. Organic Geochemistry 39, 689–710.
757 Wakeham, S.G., Canuel, E.A., 2006. Degradation and preservation of organic matter in
758 marine sediments, in: Volkman, J.K. (Ed.), Marine Organic Matter: Biomarkers,
759 Isotopes and DNA. The Handbook of Environmental Chemistry, Vol 2N. Springer
760 Berlin Heidelberg, Berlin, Heidelberg, pp. 295–321.
761 Weber, R.R., Montone, R.C., 2006. Rede 2 - Gerenciamento ambiental na Baía do
762 Almirantado, Ilha Rei George, Antártica.
763 Weijers, J.W.H., Schouten, S., Spaargaren, O.C., Sinninghe Damsté, J.S., 2006.
764 Occurrence and distribution of tetraether membrane lipids in soils: Implications for
765 the use of the TEX86 proxy and the BIT index. Organic Geochemistry 37, 1680–
766 1693.
767 Wisnieski, E., Bícego, M.C., Montone, R.C., Figueira, R.C.L., Ceschim, L.M.M.,
768 Mahiques, M.M., Martins, C.C., 2014. Characterization of sources and temporal
769 variation in the organic matter input indicated by n-alkanols and sterols in
770 sediment cores from Admiralty Bay, King George Island, Antarctica. Polar
771 Biology 37, 483–496.
772 Zhang, Y.G., Pagani, M., Wang, Z., 2016. Ring Index: A new strategy to evaluate the
773 integrity of TEX86 paleothermometry. Paleoceanography 31, 220–232.
774 Zhang, Y.G., Zhang, C.L., Liu, X.-L., Li, L., Hinrichs, K.U., Noakes, J.E., 2011.
775 Methane Index: A tetraether archaeal lipid biomarker indicator for detecting the
776 instability of marine gas hydrates. Earth and Planetary Science Letters 307, 525–
777 534.
778

779 **Figure Captions**

780

781 Fig. 1. Map of the study area with the location of the sediment cores collected in
782 Admiralty Bay, Antarctic Peninsula. The red dots represent the location of the sediment
783 cores, the blue diamonds represent glaciers mentioned in the Discussion, and the red
784 triangle represents the Russian Bellingshausen research station.

785

786 Fig. 2. Profiles and trends (based on linear models between 1963 and 1975, 1975 and
787 1998, and 1998 and 2006; dashed lines) of the total organic carbon (TOC, in %), total
788 sterols (in $\mu g\ g^{-1}$), total alcohols (in $\mu g\ g^{-1}$), and isoprenoid GDGTs (in $\mu g\ g^{-1}$) in the BTP
789 sediment core.

790

791 Fig. 3. Profiles of the main sterols, the fatty aliphatic alcohols and the main isoprenoid
792 GDGTs (all data in $\mu g\ g^{-1}$); and the ratio of 5α-stanols/Δ^5-stenols in the BTP sediment
793 core. The vertical dashed gray line indicates the threshold of diagenesis (Wakeham and
794 Canuel, 2006).

795

796 Fig. 4. Comparison between GDGT-based sea surface temperatures (SST) from our short
797 marine sediment cores and instrumental temperatures from SODA3 reanalysis. The red
798 line represents the mean austral spring (OND) temperature, while the red band represents
799 the annual variation. Regarding the GDGT-based SST estimates, the line represents the
800 calculated SST using five different calibrations (from left to right: TEX_{86}^{L}, AntPen,
801 Bayspar, TEX_{86}^{L} quad and OPTiMAL), while the bands represent the calibration errors
802 (from left to right: TEX_{86}^{L} = ± 4 °C, AntPen = ± 2.2 °C, Bayspar = ± 5 °C, TEX_{86}^{L} quad
803 = ± 5 °C and OPTiMAL = ± 3.4 °C).

804

805 Fig. 5. Profiles of the normalized proxies of organic matter (total sterols, total alcohols
806 and isoGDGTs), sea surface temperature (in °C), seasonal means of wind speed in
807 Bellingshausen (in $m\ s^{-1}$), seasonal mean of precipitation in Bellingshausen (in mm), and
808 area loss of the main glaciers around Botany Point (in km^2). The trends (colored dashed
809 lines) are based on linear models between 1963 and 1975, 1975 and 1998, and 1998 and
810 2006.

811

812 Fig. 6. Comparison between GDGT-based sea surface temperatures from Botany Point
813 (BTP) and mean annual air temperatures from King George Island based on Kejna et al.
814 (2013). (Top panel) The band represents the calibration error (± 5 °C), while the error
815 bars in the x-axis represent the age model uncertainties. (Bottom panel) Trends (based on
816 linear models) between the periods: 1963 – 1975, 1975 – 1998 and 1998 – 2006 (2011 in
817 the MAT data).
818
819 **Table Captions**
820
821 Table 1. Sediment cores collected at Admiralty Bay, King George Island, Antarctica. LSR
822 = Mean post-1963 estimated linear sedimentation rates.
823
824 Table 2. Spearman correlation analysis between GDGTs-based sea surface temperatures
825 (considering the three records combined) and mean annual and austral seasonal
826 temperatures from SODA3 reanalysis. x = *p*-value < 0.05. JFM = austral summer, AMJ
827 = austral autumn, JAS = austral winter, OND = austral spring. Calibrations: TEX_{86}^{L} based
828 on Kim et al. (2010); AntPen based on Shevenell et al. (2011); Bayspar based on Tierney
829 and Tingley (2014); TEX_{86}^{L} quad based on Park et al. (2019) and OPTiMAL based on
830 Dunkley Jones et al. (2020).

Exploring the application of TEX_{86} and the sources of organic matter in the Antarctic coastal region

Ana Lúcia L. Dauner, B. David A. Naafs, Richard D. Pancost, César C. Martins

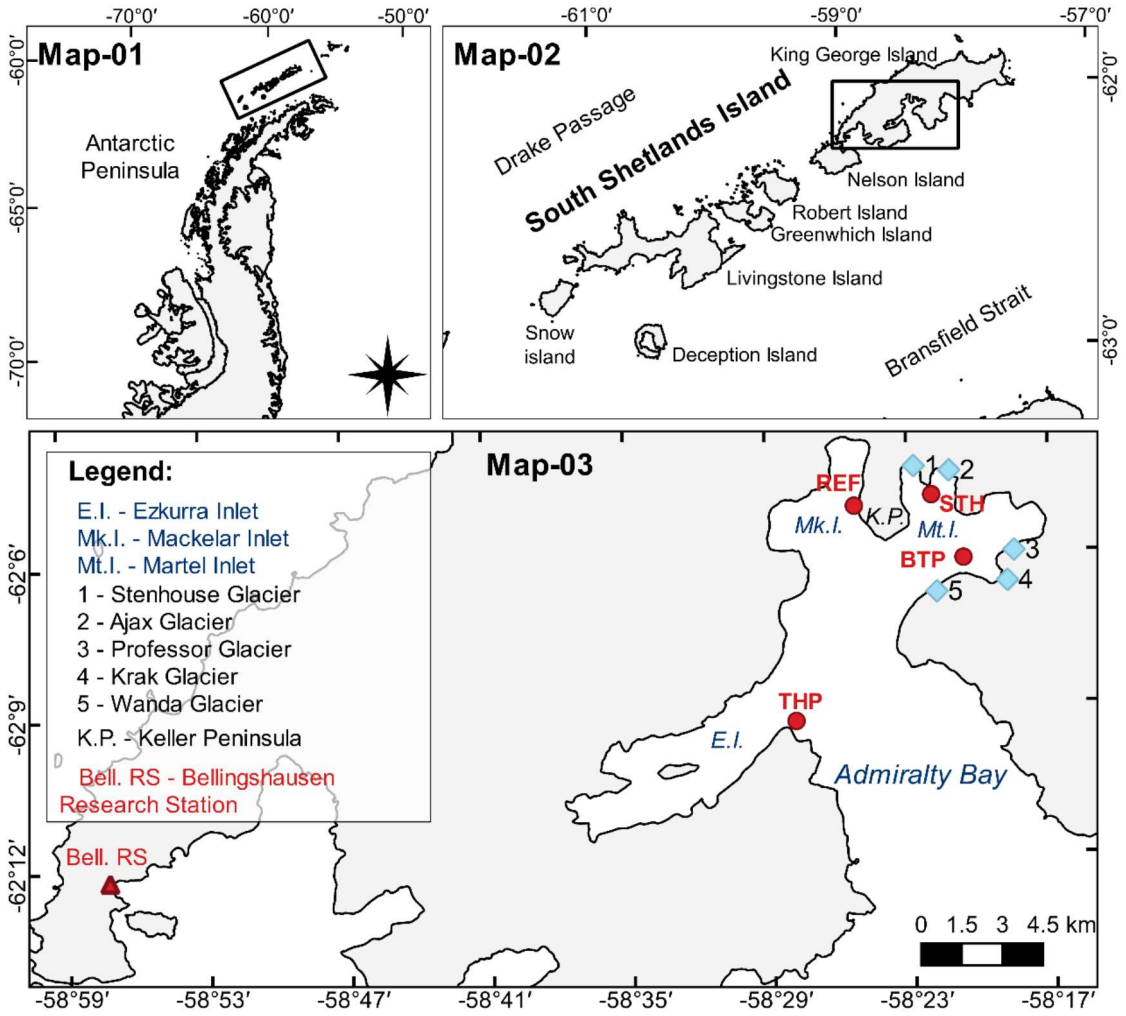

Fig. 1

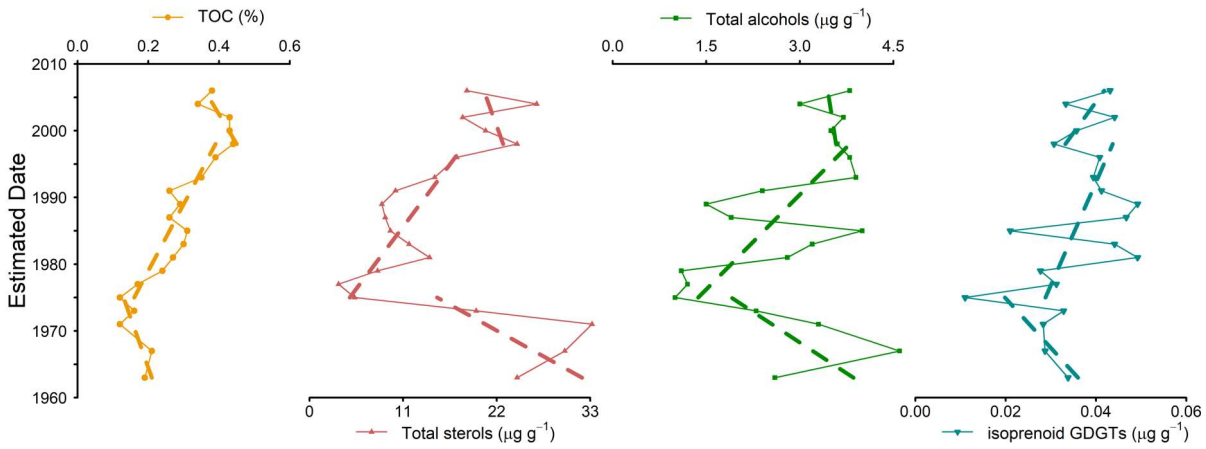
TOC (%)
0.0
0.2
0.4
0.6
Estimated Date
2010
2000
1990
1980
1970
1960
Total sterols (μg g−1)
0
11
22
33
Total alcohols (μg g−1)
0.0
1.5
3.0
4.5
isoprenoid GDGTs (μg g−1)
0.00
0.02
0.04
0.06

Fig. 2

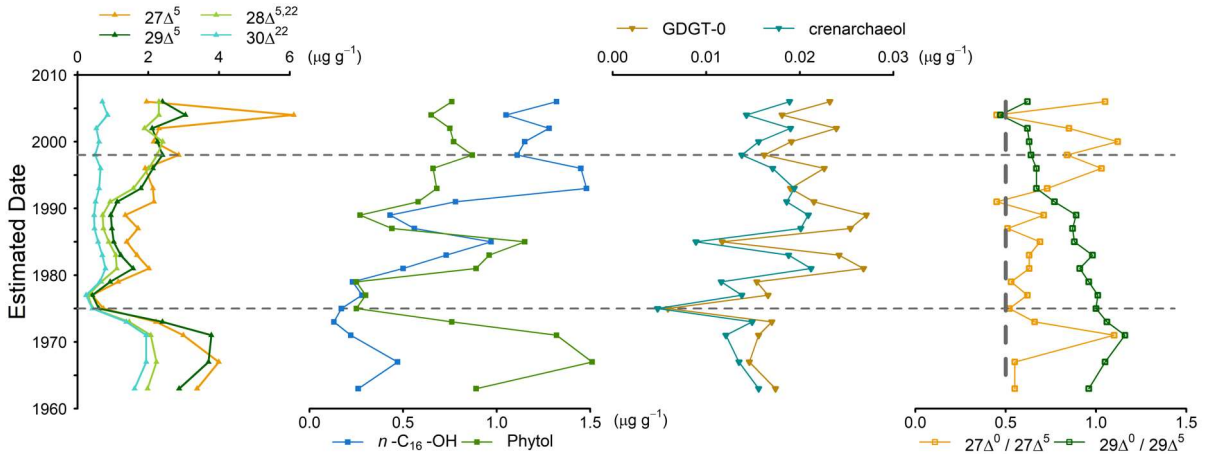
27Δ5
29Δ5
28Δ5,22
30Δ22
(μg g−1)
Estimated Date
2010
2000
1990
1980
1970
1960
n-C16-OH
Phytol
(μg g−1)
GDGT-0
crenarchaeol
(μg g−1)
27Δ0 / 27Δ5
29Δ0 / 29Δ5

Fig. 3

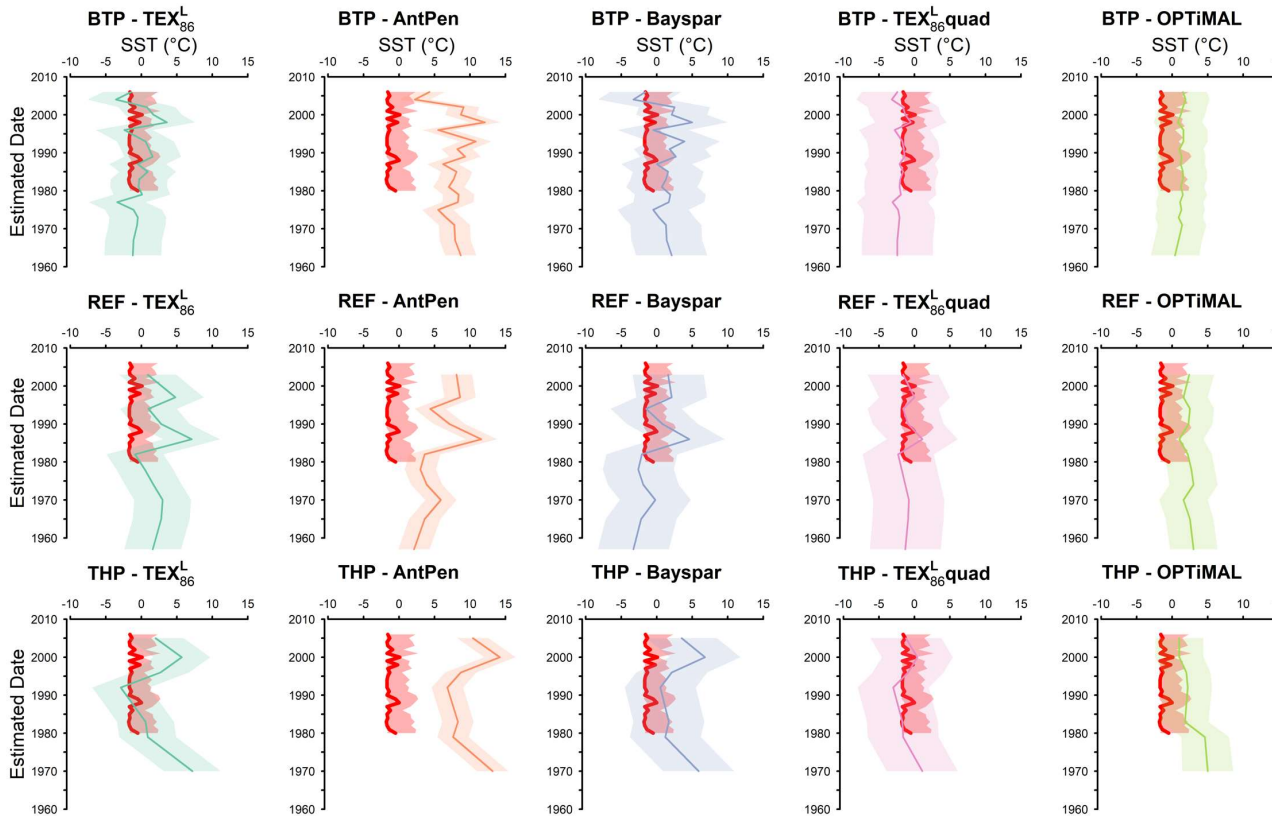
BTP - TEX$^{L}_{86}$
BTP - AntPen
BTP - Bayspar
BTP - TEX$^{L}_{86}$quad
BTP - OPTiMAL
REF - TEX$^{L}_{86}$
REF - AntPen
REF - Bayspar
REF - TEX$^{L}_{86}$quad
REF - OPTiMAL
THP - TEX$^{L}_{86}$
THP - AntPen
THP - Bayspar
THP - TEX$^{L}_{86}$quad
THP - OPTiMAL
SST (°C)
Estimated Date

Fig. 4

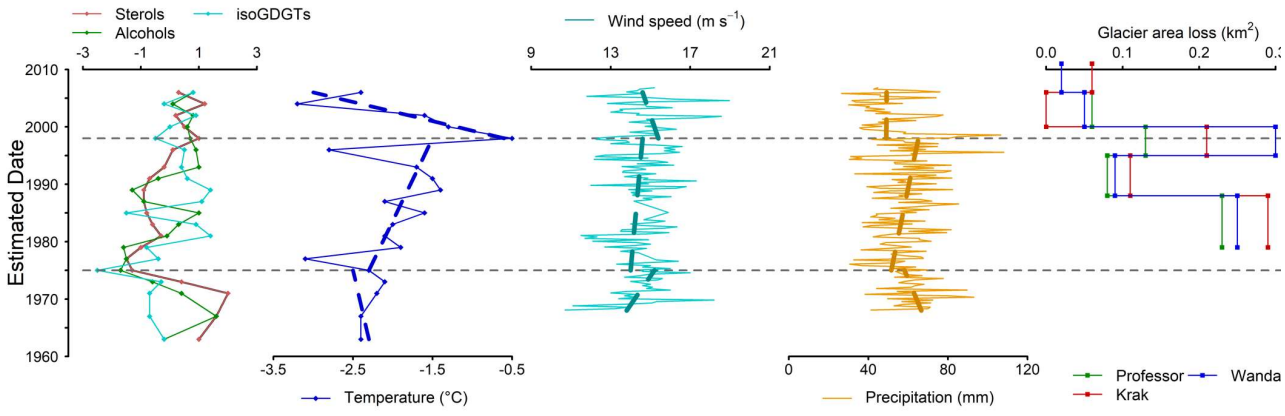
Sterols
Alcohols
isoGDGTs
Wind speed (m s^{-1})
Glacier area loss (km^2)
Estimated Date
Temperature (°C)
Precipitation (mm)
Professor
Wanda
Krak

Fig. 5

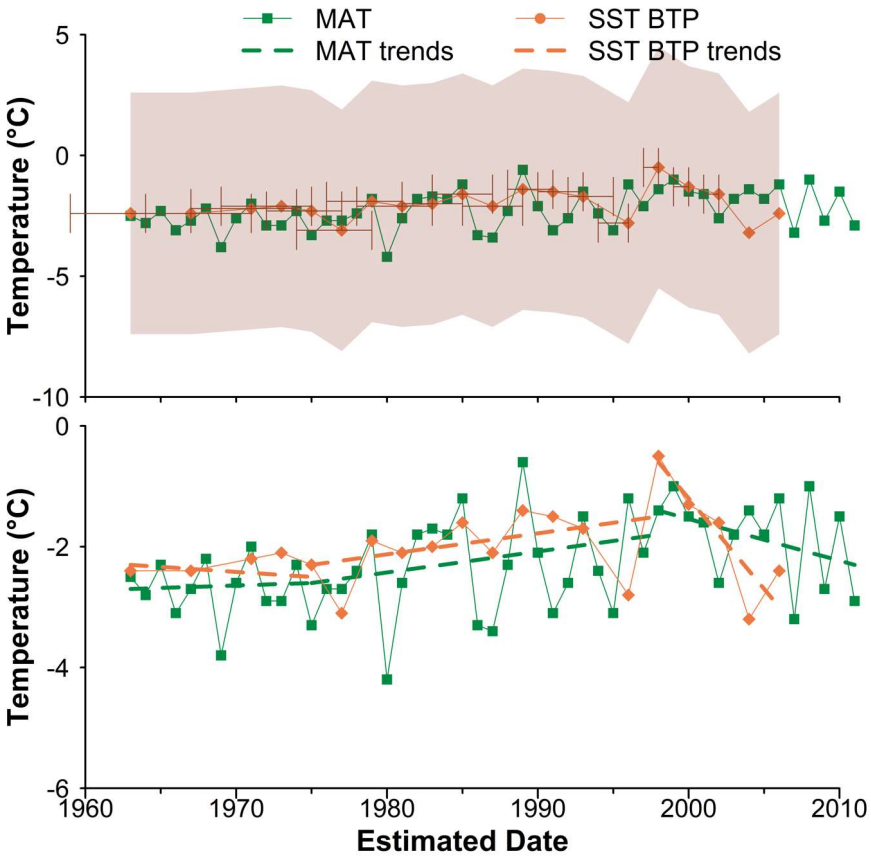
MAT
MAT trends
SST BTP
SST BTP trends
Temperature (°C)
5
0
-5
-10
Temperature (°C)
0
-2
-4
-6
1960
1970
1980
1990
2000
2010
Estimated Date

Fig. 6

Exploring the application of TEX_{86} and the sources of organic matter in the Antarctic coastal region

Ana Lúcia L. Dauner, B. David A. Naafs, Richard D. Pancost, César C. Martins

Table 1. Sediment cores collected at Admiralty Bay, King George Island, Antarctica. LSR = Mean post-1963 estimated linear sedimentation rates.

Site	Name	Latitude	Longitude	Depth (m)	LSR (cm yr^{-1})
BTP	Botany Point	- 62.09718	- 58.35078	30	0.48 [a]
REF	Refuge II	- 62.07952	- 58.42745	20	0.26 [b]
STH	Stenhouse Glacier	- 62.07625	- 58.37270	25	0.42 [a]
THP	Thomas Point	- 62.15040	- 58.47140	20	0.23 [b]

[a] Ferreira et al. (2013); [b] Martins et al. (2014)

Table 2. Spearman correlation analysis between GDGTs-based sea surface temperatures (considering the three records combined) and mean annual and austral seasonal temperatures from SODA3 reanalysis. x = *p*-value < 0.05. JFM = austral summer, AMJ = austral autumn, JAS = austral winter, OND = austral spring. Calibrations: TEX_{86}^{L} based on Kim et al. (2010); AntPen based on Shevenell et al. (2011); Bayspar based on Tierney and Tingley (2014); TEX_{86}^{L} quad based on Park et al. (2019) and OPTiMAL based on Dunkley Jones et al. (2020).

Calibration	Annual	JFM	AMJ	JAS	OND
TEX_{86}^{L}	x	x	x	x	0.54
AntPen	x	- 0.44	x	x	0.61
Bayspar	x	- 0.44	x	x	0.61
TEX_{86}^{L} quad	x	x	x	x	0.56
OPTiMAL	x	x	x	x	- 0.60